Original Article

Diagnostic accuracy of contrast-enhanced dual-energy computed tomography for detecting metastatic lymph nodes in patients with malignant tumors: a systematic review and meta-analysis

Derui Kong[1#], Xinyu Chen[2#], Peihong Gao[1], Kexin Zhao[1], Chong Zheng[1], Hongwei Zhou[1]

[1]Department of Radiology, First Hospital of Jilin University, Changchun, China; [2]Department of Anesthesiology, First Hospital of Jilin University, Changchun, China

Contributions: (I) Conception and design: D Kong, X Chen; (II) Administrative support: H Zhou, P Gao; (III) Provision of study materials or patients: K Zhao; (IV) Collection and assembly of data: C Zheng; (V) Data analysis and interpretation: D Kong; (VI) Manuscript writing: All authors; (VII) Final approval of manuscript: All authors.

[#]These authors contributed equally to this work.

Correspondence to: Hongwei Zhou, MD. Department of Radiology, First Hospital of Jilin University, #71 Xinmin St., Changchun 130021, China. Email: hwzhou@jlu.edu.cn.

Background: This meta-analysis evaluated the diagnostic accuracy of contrast-enhanced dual-energy computed tomography (DECT) for detecting metastatic lymph nodes in patients with cancer.

Methods: PubMed, Embase and Cochrane Library databases were searched for literature published from database inception until September 2022. Only studies that investigated the diagnostic accuracy of DECT for metastatic lymph nodes in patients with malignant tumors and surgically removed metastatic lymph nodes for pathological confirmation were included. The quality of the included studies was evaluated using the Quality Assessment of Diagnostic Accuracy Studies tool. The threshold effect was determined by calculating Spearman correlation coefficients and summary receiver operating characteristic (SROC) curve patterns. Deeks test was used to assess publication bias.

Results: All of the included studies were observational studies. A total of 16 articles involving 984 patients were included (2,577 lymph nodes) in this review. A total of 15 variables were included in the meta-analysis, including 6 individual parameters and 9 combined parameters. Normalized iodine concentration (NIC) in the arterial phase combined with the slope in the arterial phase showed better identification of metastatic lymph nodes. The spearman correlation coefficient was –0.371 (P=0.468), and the SROC curve did not show a "shoulder-arm" shape, suggesting that there was no threshold effect and that heterogeneity was present. The combined sensitivity was 94% [95% confidence interval (CI): 86–98%], the specificity was 74% (95% CI: 52–88%), and the area under the curve was 0.94. The Deeks test suggested no significant publication bias in the included studies (P=0.06).

Conclusions: NIC in arterial phase combined with the slope in the arterial phase has some diagnostic value in differentiating between metastatic and benign lymph nodes, but this should be further evaluated in additional studies with rigorous design and high homogeneity.

Keywords: Radiography; dual-energy computed tomography (DECT); metastatic lymph nodes; cancer

Submitted May 26, 2022. Accepted for publication Dec 27, 2022. Published online Feb 09, 2023.
doi: 10.21037/qims-22-527
View this article at: https://dx.doi.org/10.21037/qims-22-527

Introduction

In most countries, cancer is the primary cause of mortality before the age of 70 years and a major impediment to extending life expectancy. According to figures from the International Agency for Research on Cancer (IARC), 19.3 million new cancer cases and approximately 10 million deaths were estimated to occur globally in 2020 (1). The main purpose of lymph node assessment is the staging of the cancer, which is important in the choice of treatment options. Lymph nodes serve as conduits for the spread of cancer to other organs in many different forms of cancer. Lymph node metastasis is an essential prognostic characteristic and one of the most important determinants impacting patient survival (2). Therefore, accurate detection of lymph node metastases is critical for cancer staging and treatment planning (3).

In recent years, dual-energy computed tomography (DECT) has been widely used for the prediction of various types of cancer and other diseases such as lung cancer (4), gastrointestinal tumors (5), breast cancer (6), biliary tract cancer (7), adherent perinephric fat (8), microthrombosis associated with COVID-19 pneumonia (9), pulmonary emboli (10), and lumbar disk herniation (11). DECT is a CT technique that uses two different X-ray energies, and it can accurately determine the composition of objects, thereby substantially increasing the capabilities of traditional CT single-energy scanning (12).

The difference between contrast-enhanced CT and traditional CT is that contrast-enhanced CT uses intravenous iodine contrast to assess whether there is blood perfusion. When the contrast is injected in the blood stream and shows perfusion, this is crucial since perfusion is a hallmark of cancer. Contrast-enhanced DECT can provide an iodine map to assess the iodine content of the tissue and indirectly reflect the blood supply to the tissue (13). In addition to traditional CT images, DECT can provide monochromatic images at 40–200 keV energy levels (14), iodine concentration (IC) mapping, effective atomic number (effc-z) images, and many other quantitative parameters, making it a significant milestone for CT diagnosis (4-11,15). DECT has shown promise in the diagnosis of preoperative metastatic lymph nodes in recent years (16), and DECT characteristics may help to distinguish metastatic from benign lymph nodes (17).

Different manufacturers often apply different DECT imaging techniques, which can be broadly divided into two categories: (I) one based on the detector side of the approach, such as detector-based DECT, which has 2 layers of detectors that detect low versus high energy photons and (II) another based on the tube sphere side of the approach, such as dual-source DECT, single-source DECT with rapid kilovoltage switching, and split-beam DECT (18). The differences of these technologies mainly stem from the product characteristics of different manufacturers and the different implementation forms of energy scanning (19). Each of these techniques has its own characteristics. To date, there is no consensus on which manufacturer and which technique provides the best diagnostic performance (20).

Furthermore, no systematic assessments or meta-analyses have been conducted on the usefulness of DECT in the detection of metastatic lymph nodes. Therefore, this review includes a large number of studies relevant to the topic. This allowed for an assessment of the sensitivity and specificity of DECT for lymph node metastasis. The following article is presented in accordance with the PRISMA-DTA reporting checklist (available at https://qims.amegroups.com/article/view/10.21037/qims-22-527/rc).

Methods

The PRISMA-DTA standards were used to conduct this systematic review and meta-analysis, which follows current best practices (21). Prior to the start of the review, the systematic review was prospectively registered and submitted to the PROSPERO database (CRD42022303023). This meta-analysis was not subject to ethical approval.

Search strategy

A comprehensive search of the PubMed, Embase, and Cochrane Library databases was performed for literature published in the English language from the inception of each database to September 30, 2022. Preliminary keywords and medical subject headings (MeSH) terms, including lymph nodes, metastatic lymph nodes, spectral CT, dual energy, and CT, were combined to generate a list of studies. The search strategy is shown in Appendix 1.

Selection of studies

After eliminating duplicates, the abstract and title of the remaining articles were independently screened by two investigators according to the inclusion and exclusion criteria. When a study was deemed eligible, the full text

was obtained, and further screening was performed. Once agreement between the two investigators (ZKX and ZC) was reached, the final list of studies underwent full-text analysis and data extraction. When there was disagreement between raters, a consensus was reached through discussion or consultation with a third investigator (KDR).

Full-text articles were thoroughly selected according to the following inclusion criteria: (I) inclusion of patients with malignant neoplasms; (II) the application of DECT in the detection of metastatic lymph nodes; (III) surgical removal of metastatic lymph nodes for pathological confirmation; and (IV) the assessment of the diagnostic accuracy of lymphatic metastasis with DECT, with the data permitting the construction of a 2×2 table for calculating the diagnostic accuracy of DECT, including true positive (TP), false positive (FP), false negative (FN), and true negative (TN) results. Publications were excluded if they met any of the following criteria: (I) a lack of blood supply for the primary tumor; (II) inability to obtain the full text and extract data or the diagnostic indicators for individual parameters; (III) lack of reporting for the outcome of tumor recurrence; (IV) non-English language literature; and (V) reviews, retrospective studies, conference abstracts, case report/case series, and meta-analyses.

Data extraction

Two investigators (KDR and CXY) independently extracted data from the identified studies. When the data information in the original articles was unclear or the two investigators had different opinions, differences were resolved through discussion.

The following characteristics were extracted: study characteristics, including first author, year of publication, prospective versus retrospective study design, total number of patients, mean age, number and percentage of males, type of disease, total number of lymph nodes, and number of metastatic lymph nodes; and DECT characteristics, including machine brand, DECT type, tube voltage, tube current, slice thickness (mm), collimation (mm), rotation time (s), and contrast time (s). Finally, the true-positive, false-positive, true-negative, and false-negative rates (%), as well as sensitivity and specificity of identifying metastatic lymph nodes were reported. If they were not explicitly stated in the original research, data on TPs, FPs, TNs, and FNs were estimated based on the number, sensitivity, and specificity of lymph nodes described in the literature.

Assessment of methodological quality

Two investigators (GPH and ZHW) independently assessed the methodological quality of the included studies using the Quality Assessment of Diagnostic Accuracy Studies 2 (QUADAS-2) tool (22), and differences were addressed by consensus. If no consensus was achieved between the 2 raters, a third rater (KDR) was consulted.

Statistical analysis and data synthesis

If the parameters included in this analysis had different degrees of heterogeneity, different cutoff values could have led to different sensitivities and specificities of diagnostic tests, and a threshold effect would be generated. Therefore, we first tested whether there was a threshold effect for the diagnostic test. To determine whether there was a threshold effect, Spearman correlation coefficient and summary receiver operating characteristic (SROC) curves were used. If there was a positive correlation between sensitivity and specificity ($P<0.05$) or the scatter points in the SROC curve showed a "shoulder-arm" distribution, heterogeneity caused by a threshold effect was considered. Conversely, if there was no positive correlation between sensitivity and specificity ($P>0.05$) or the scatter points in the SROC curve showed a "non-shoulder arm" distribution, there was considered to be was no threshold effect leading to heterogeneity. If there was a threshold effect, the best method to merge data was to fit the SROC curve and to calculate the area under the ROC curve, or not to merge the data. If there was no threshold effect, the effect values were combined. The effect model depended on whether there was heterogeneity between the studies.

The I^2 test [$I^2=100\% \times (Q-df)/Q$] was used to assess heterogeneity of the studies that were included in the meta-analysis. Each parameter was statistically assessed using Stata 15.0 (StataCorp LLC, College Station, TX, USA) and Meta-Disc 14.0 (https://meta-disc.software.informer.com/1.4/). The effect size included sensitivity, specificity, positive likelihood ratio, negative likelihood ratio (NLR), diagnostic advantage ratio, and area under the SROC curve (AUC). If $I^2 \leq 50\%$ or $P>0.05$ showed that there was no substantial heterogeneity, the fixed effects model was employed to combine the effect indicators. If $I^2>50\%$ or $P<0.05$, a random effects model was used to combine effect indicators, and sensitivity and heterogeneity tests were performed. A forest plot was also generated to show the

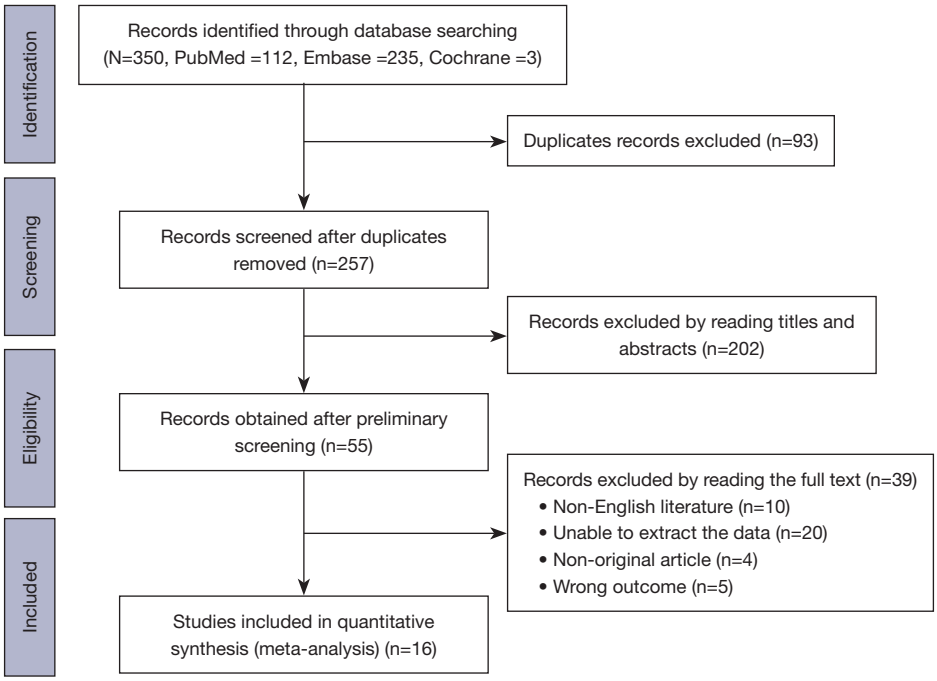

Figure 1 Flow diagram showing the study selection process for the meta-analysis.

results of the data synthesis.

To perform sensitivity analyses, Stata software was used. The software examined the effect of a single study on the pooled effect size by observing whether the results changed significantly after removal of a particular study. Finally, Deeks test was employed to examine publication bias, with $P<0.05$ indicating the presence of publication bias.

Results

Literature search

A total of 350 relevant papers were obtained by searching the databases, and after deduplication, 257 original studies were identified. After a reading of the titles and abstracts of these 257 original studies, 202 papers were excluded. Then, full texts were read in detail, and a rescreening was performed based on the inclusion and exclusion criteria, resulting in a final sample of 16 eligible studies for inclusion in this meta-analysis (16,23-37). The flowchart outlining the screening process is shown in *Figure 1*. The specific reasons for exclusion at the full-text screening stage are described in the Appendix 2.

Study characteristics

This meta-analysis included 16 original investigations, totaling 2,577 lymph nodes from 984 individuals. The papers included were published between 2015 and 2022, with 11 studies having been published in the last 5 years (16,23-32). The mean age of patients in the 16 included studies varied from 34.0±7.8 to 59.5±8.7 years, while the percentage of males ranged from around 0.0% to 70.9%. Moreover, 7 of the 16 studies included patients with thyroid cancer (16,23,24,29,30,33,36), 4 studies included patients with colorectal cancer (25,28,35,37), and the remaining 5 studies included patients with esophageal cancer, liver cancer, breast cancer, squamous cell carcinoma of the oropharynx, or lung cancer (26,27,31,32,34). *Table 1* details the patient characteristics of the included studies. *Table 2* details the DECT characteristics of the listed studies. Regarding manufacturer type, 6 studies used Siemens equipment, 9 nine studies used General Electric Company equipment. The majority of studies used dual-energy X-rays at energies of 80 to 140 kV. Of the studies included, 4 used single-energy DECT while 9 used dual-energy DECT, and the technology employed in the remaining 3 studies was not

Table 1 Characteristics of the studies included in this meta-analysis

Reference	Year	Study type	Number of patients	Age (years)	Sex (% male)	Cancer type	Total number of LNs	Total number of MLNs
Zou *et al.* 2021	2021	Retrospective study	52	43.00±15.22	11 (21.2)	Papillary thyroid carcinoma	359	139
Zhuo *et al.* 2021	2021	Retrospective study	74	N	40 (54.1)	Papillary thyroid carcinoma	216	92
Wu *et al.* 2021	2021	Controlled study	35	39.79±13.58	6 (17.1)	Papillary thyroid carcinoma	206	80
Qiu *et al.* 2021	2021	Prospective study	71	59.3±14.1	41 (57.7)	Colorectal cancer	150	84
Sun *et al.* 2020	2020	Retrospective study	26	N	N	Esophageal cancer	51	34
Zeng *et al.* 2019	2019	Retrospective study	43	N	N	Hepatocellular carcinoma	156	52
Yang *et al.* 2019	2019	Prospective study	178	55.59±12.87	119 (66.9)	Colorectal cancer	178	72
Li *et al.* 2019	2019	Retrospective study	30	41.6±14.8	13 (43.3)	Papillary thyroid carcinoma	99	70
He *et al.* 2019	2019	Prospective study	51	N	16 (31.4)	Papillary thyroid carcinoma	212	124
Zhang *et al.* 2018	2018	Prospective study	193	47.6±10.1	0 (0.0)	Breast cancer	337	76
Foust *et al.* 2018	2018	Retrospective study	8	N	N	Squamous cell carcinoma of the oropharynx	29	13
Zhao *et al.*2017	2017	Retrospective study	34	42.24±14.65	16 (47.1)	Papillary carcinoma and medullary carcinoma	136	102
Li *et al.* 2016	2016	Retrospective study	61	59.5±8.7	37 (60.7)	Lung cancer	40	20
Liu *et al.* 2015	2015	Prospective study	45	34.0±7.8	11 (24.4)	Papillary thyroid carcinoma	175	63
Liu *et al.* 2015	2015	Prospective study	55	N	39 (70.9)	Colorectal cancer	152	60
Kato *et al.* 2015	2015	Retrospective study	28	N	N	Colorectal cancer	81	35

The data of age are expressed as mean ± standard deviation. N, not reported; LN, lymph node; MLN, metastatic lymph node.

specified.

Methodological quality

We used the QUADAS-2 tool to evaluate the quality of primary diagnostic accuracy studies, and *Figure 2* summarizes the overall risk of bias and applicability concerns for this research.

For the diagnostic experiments to be evaluated (whether or not predetermined thresholds were used in the original studies), we judged the risk of bias for diagnostic experiments to be evaluated (QUADAS-2, domain 2) to be high in all studies. We assessed the risk of bias by determining whether there was a time interval between the diagnostic experiment and the gold standard (QUADAS-2, domain 4). In 11 of the 16 studies included, the time interval between the DECT examination and the pathological gold standard was not clearly stated, and, therefore, the risk of bias was considered to be unclear for these 11 articles. The evaluation of clinical applicability included the selection of cases, the implementation and interpretation of the experiments, and the evaluation of the applicability of the gold standard.

Results of data synthesis

Value of each parameter of DECT in the diagnosis of metastatic lymph nodes

Due to the small amount of studies on some parameters, the diagnostic performance of only 15 indicators was analyzed.

Table 2 Dual-energy CT characteristics of the individual included studies

Reference	DECT brand	DECT type	kV1	kV2	Tube current	Slice thickness (mm)	Collimation	Rotation time (s)	Contrast	Dose	Flow rate	Arterial phase (s)	Venous phase (s)
Zou *et al.* 2021	Siemens	Dual source	N	N	600 mA	1	64 mm ×0.6 mm	N	Iohexol	1 mL/kg	3 mL/s	25	45
Zhuo *et al.* 2021	Siemens	Dual source	90	150	250 mA, 125 mA	0.75	2 mm ×192 mm ×0.6 mm	0.5	Iopromide	N	4 mL/s	N	50
Wu *et al.* 2021	GE	Single source fast switching kV	80	140	260 mA	1.25	N	N	Iohexol 350	1.2 mL/kg	3.1 mL/s	N	50
Qiu *et al.* 2021	Canon	Single source fast switching kV	80	135	112–187 mA	0.5	N	N	Ultravist 300	1.0 mL/kg	3 mL/s	40	70
Sun *et al.* 2020	Siemens	N	90	150	N	1	N	0.25	Iohexol	N	23 mgI/kg/s	N	N
Zeng *et al.* 2019	GE	Single source fast switching kV	80	140	600 mA	1.25	N	0.8	Ioversol 320	1.0 mL/kg	3.0 mL/s	25	65
Yang *et al.* 2019	GE	Single source fast switching kV	80	140	375 mA	1.25	N	N	Iohexol	1.5 mL/kg	4ml/s	N	N
Li *et al.* 2019	GE	Single source fast switching kV	80	140	260 mA	5	N	0.7	N	N	3.0 mL/s	N	45
He *et al.* 2019	Siemens	Dual source	80	150	130 mA, 65 mA	1.5	128 mm ×0.6 mm	1	Ioversol 370	85 mL	3.0 mL/s	N	30
Zhang *et al.* 2018	GE	N	N	N	275 mA	1.25	N	N	Iohexol	1.5 mL/kg	4 mL/s	N	N
Foust *et al.* 2018	Siemens	Dual source	80	140	302 mA, 157 mA	0.75	0.6 mm	0.28	N	50 mL	3 mL/s	N	35
Zhao *et al.*2017	GE	Single source fast switching kV	80	140	260 mA	5	N	0.7	N	90 mL	3.0 mL/s	N	45
Li *et al.* 2016	GE	Single source fast switching kV	80	140	N	1.25	N	N	Iohexol	1.2 mL/kg	2.5mL/s	N	N

Table 2 (*continued*)

Table 2 (*continued*)

Reference	DECT brand	DECT type	kV1	kV2	Tube current	Slice thickness (mm)	Collimation	Rotation time (s)	Contrast	Dose	Flow rate	Arterial phase (s)	Venous phase (s)
Liu *et al.* 2015	GE	Single source fast switching kV	N	N	550 mA	1.25	0.625 mm	N	Iopamidol 300	N	4 mL/s	25	50
Liu *et al.* 2015	GE	Single source fast switching kV	80	140	600 mA	1.25	N	0.6	Ultravist	1.5 mL/kg	3 mL/s	N	N
Kato *et al.* 2015	Siemens	N	N	N	N	N	N	N	N	N	N	44	70

CT, computed tomography; DECT, dual-energy computed tomography; GE, GE Healthcare; kV, kilovoltage; N, not reported.

The data on the TPs, FPs, TNs, FNs, sensitivities, and specificities of each parameter, as well as main characteristics, are shown in Appendix 3. Each parameter included in the analysis had varying degrees of heterogeneity (available online: https://cdn.amegroups.cn/static/public/qims-22-527-1.pdf). The effect sizes of the diagnostic sensitivity, specificity, positive likelihood ratio, NLR, diagnostic ratio, and area under the SROC curve (AUC) are summarized for each parameter of DECT in *Table 3*.

As can be seen from the summary in *Table 3*, of the 15 parameters, 4 had relatively large AUC values of 90% or more. These were normalized iodine concentration (NIC) in the arterial phase combined with the slope in the arterial phase, NIC in the arterial phase combined with NIC in the venous phase, NIC in the arterial phase combined with the slope in the venous phase, and the slope in the arterial phase combined with the slope in the venous phase, and their corresponding AUC values were 0.94, 0.90, 0.93, and 0.93, respectively. The sensitivity and specificity of NIC in the arterial phase combined with the slope in the arterial phase were 94% (95% CI: 86–98%) and 74% (95% CI: 52–88%) (*Figure 3*), respectively, with a large amount of heterogeneity in sensitivity (I^2=88.96%) and specificity (I^2=97.36%). The combined positive likelihood ratio (PLR) was 3.39 (95% CI: 2.22–5.18) (*Figure 4A*), the combined NLR was 0.10 (95% CI: 0.04–0.27) (*Figure 4B*), and the combined diagnostic odds ratio (DOR) was 38.86 (95% CI: 9.00–167.66) (*Figure 4C*). Among all the parameters, the AUC of NIC in the arterial phase combined with the slope in the arterial phase was the largest, with a value of 0.94 (*Figure 4D*).

Threshold effect

The results are shown in *Table 3*; the SROC curve lacked a shoulder-arm structure, suggesting that no threshold effect existed. After excluding the effect of threshold effects, we also considered the heterogeneity caused by non-threshold effects.

Since there was no threshold effect in this study, the presence of heterogeneity was deemed not to be related to the threshold effect. Therefore, this study used a random effects model to combine effect sizes and analyze the sources of heterogeneity.

Sensitivity analysis

The above effect size synthesis and data analysis found that the NIC in the arterial phase combined with slope in the arterial phase had the highest AUC. We focused on the sensitivity analysis of this combination. As shown in *Figure 5*, regardless of which study was excluded, the final combined result was not significantly affected, indicating that each study had little influence on the general results. As such, the results of this study were stable. We also examined sensitivity analysis results for other parameter combinations, which are shown in https://cdn.amegroups.cn/static/public/qims-22-527-2.pdf, and these results were all stable.

Figure 2 Risk of bias and applicability concerns for the studies included in the meta-analysis. (A) Risk of bias summary. (B) Risk of bias graph.

Investigation of heterogeneity

Sources of clinical variability were explored by meta-regression. Based on clinical practice, we then formally evaluated the effects of the following variables on sensitivity and specificity: DECT manufacturers (Siemens *vs.* General Electric Company), blood supply (abundant *vs.* insufficient), contrast flow rate (>3 *vs.* ≤3 mL/s), and study design (prospective *vs.* retrospective). The results of the meta-regression for each parameter are shown in *Table 4*. For the NIC in the arterial phase combined with the slope in the arterial phase, meta-regression analysis showed a significant effect of experimental design on the heterogeneity of sensitivity.

Table 3 Combined effect size of each parameter of dual-energy computed tomography

Parameter	Sensitivity	Specificity	PLR	NLR	DOR	AUC	Spearman correlation	P value
IC in AP	0.77 (0.70–0.83)	0.78 (0.70–0.84)	3.42 (2.32–5.04)	0.3 (0.22–0.43)	12.01 (5.73–25.16)	0.84	–0.429	0.397
NIC in AP	0.78 (0.69–0.86)	0.79 (0.66–0.88)	3.49 (2.19–5.57)	0.29 (0.19–0.46)	13.74 (5.48–34.45)	0.85	–0.042	0.907
Slope in AP	0.74 (0.65–0.82)	0.85 (0.72–0.93)	4.12 (2.50–6.77)	0.32 (0.22–0.47)	13.82 (6.46–25.96)	0.85	–1.017	0.819
IC in VP	0.80 (0.73–0.86)	0.84 (0.79–0.88)	4.58 (3.52–5.98)	0.23 (0.15–0.36)	21.89 (11.90–40.28)	0.86	–0.429	0.289
NIC in VP	0.83 (0.74–0.89)	0.78 (0.74–0.82)	3.54 (2.93–4.26)	0.24 (0.18–0.34)	15.85 (10.21–24.63)	0.85	0.098	0.762
Slope in VP	0.75 (0.66–0.83)	0.87 (0.79–0.92)	5.26 (3.59–7.72)	0.29 (0.22–0.39)	20.75 (11.63–37.04)	0.88	0.345	0.308
IC in AP + NIC in AP	0.95 (0.78–0.99)	0.66 (0.44–0.82)	2.59 (1.76–3.81)	0.11 (0.02–0.51)	21.00 (11.69–37.70)	0.88	0.7	0.188
NIC in AP + slope in AP	0.94 (0.86–0.98)	0.74 (0.52–0.88)	3.52 (1.99–6.24)	0.10 (0.04–0.27)	38.86 (9.00–167.66)	0.94	–0.371	0.468
NIC in AP + NIC in VP	0.95 (0.91–0.98)	0.60 (0.49–0.70)	2.4 (1.84–3.13)	0.09 (0.05–0.18)	29.54 (12.78–68.27)	0.9	0	1
NIC in AP + slope in VP	0.93 (0.88–0.97)	0.73 (0.57–0.84)	3.39 (2.22–5.18)	0.10 (0.05–0.21)	37.02 (13.05–105.02)	0.93	–0.086	0.872
Slope in AP + NIC in VP	0.95 (0.89–0.97)	0.66 (0.56–0.75)	2.75 (2.05–3.68)	0.09 (0.04–0.20)	31.89 (13.69–74.24)	0.88	0.029	0.957
Slope in AP + slope in VP	0.92 (0.88–0.95)	0.74 (0.61–0.83)	3.25 (2.40–4.41)	0.12 (0.07–0.19)	32.00 (15.04–68.09)	0.93	0.036	0.939
IC in VP + NIC in VP	0.97 (0.92–0.99)	0.69 (0.62–0.75)	2.97 (2.42–3.65)	0.05 (0.02–0.15)	53.29 (20.16–140.83)	0.82	–0.072	0.878
Slope in VP + slope in VP	0.96 (0.89–0.99)	0.68 (0.61–0.74)	2.85 (2.17–3.75)	0.07 (0.03–0.20)	41.03 (14.83–113.54)	0.77	–0.486	0.329
NIC in VP + slope in VP	0.95 (0.90–0.97)	0.68 (0.62–0.74)	2.94 (2.48–3.48)	0.10 (0.06–0.17)	31.23 (18.39–53.04)	0.85	0.433	0.244

PLR, positive likelihood ratio; NLR, negative likelihood ratio; DOR, diagnostic odds ratio; AUC, area under curve; IC, iodine concentration; AP, arterial phase; NIC, normalized iodine concentration; VP, venous phase.

Publication bias

The Deeks test with Stata software was used to examine publication bias; P>0.05 indicated that there was no substantial publication bias in the included papers. *Figure 6* shows the publication bias test for NIC in the arterial phase combined with the slope in the arterial phase. The publication bias tests for the remaining parameters are shown in https://cdn.amegroups.cn/static/public/qims-22-527-3.pdf.

Discussion

Metastatic lymph nodes are the key to predicting the prognosis of cancer, and early detection of metastatic lymph nodes can help with the staging and treatment of cancer (38). DECT provides more quantitative parameters than does traditional CT, while also providing quantitative indicators, especially IC (39). This study focused on the influence of various parameters provided by an iodine map and the slope of the energy spectrum curve in the diagnosis of metastatic lymph nodes. IC and NIC can reflect the difference in iodine content between benign and malignant lymph nodes, and, thus, indirectly reflect the blood supply. Additionally, NIC avoids the effect of individual differences, and previous studies have found higher NIC values in metastatic lymph nodes than in benign lymph nodes. This is probably because tumor cells release a large number of regulatory factors before metastasis occurs, thus, stimulating the proliferation of blood vessels and lymphatic vessels in the lymph nodes

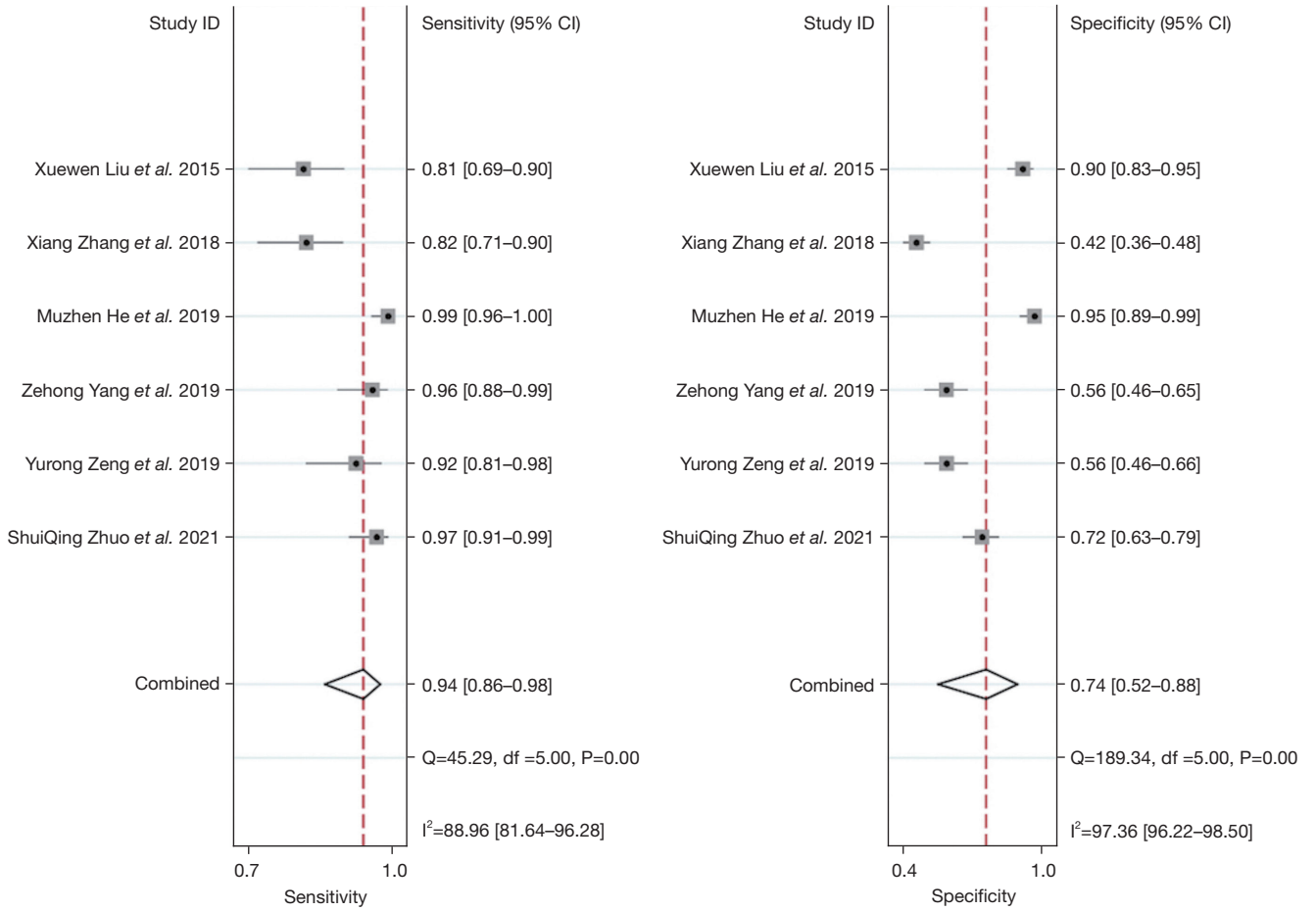

Figure 3 Forest plots of primary study sensitivity (left) and specificity (right) of the NIC in the arterial phase combined with the slope in the arterial phase for detecting metastatic lymph nodes. Each solid square represents an individual study. Error bars represent 95% CIs. Diamonds indicate the pooled sensitivity and specificity for all of the studies. NIC, normalized iodine concentration; CI, confidence interval.

which results in a widening of the microvasculature and an increase in blood flow (40). Both metastatic and no-metastatic lymph nodes follow a descending spectrum curve patterns, but the curve pattern of the metastatic nodes is much steeper, suggesting that the slope of the spectral Hounsfeld unit curve [λHU = (CT value (40 keV) – CT value (100 keV)]/(100–40). "CT value (40 keV)" and "CT value (100 keV)" are the CT attenuation measurements at 40 and 100 keV, respectively] could reflect the different statuses of lymph nodes (metastatic or non-metastatic) (37).

A total of 16 publications were included in this study comprising 2,577 lymph nodes, with disease types including thyroid cancer, lung cancer, colorectal cancer, oropharyngeal squamous cell carcinoma, breast cancer, esophageal cancer, and liver cancer,. Of the 15 indicators included in the analysis, 4 of the combined ones had a good diagnostic effect with an AUC greater than or equal to 0.90 (NIC in the arterial phase combined with slope in the arterial phase, NIC in the arterial phase combined with NIC in the venous phase, NIC in the arterial phase combined with slope in the venous phase, and slope in the arterial phase combined with slope in the venous phase). The combination of the two parameters of NIC in the arterial phase and the slope in the arterial phase not only increases the sensitivity but also has a high specificity. For this combination, the diagnostic energy efficiency analysis included 6 studies involving 1,274 lymph nodes. The sensitivity was 94%, the specificity was 74%, the AUC value of the included studies was 0.94, and the Q* value was 0.93, suggesting that the NIC in the arterial phase combined with the slope in the arterial phase has good diagnostic value for the diagnosis of metastatic lymph nodes. Moreover, to a certain extent, it avoids the missed

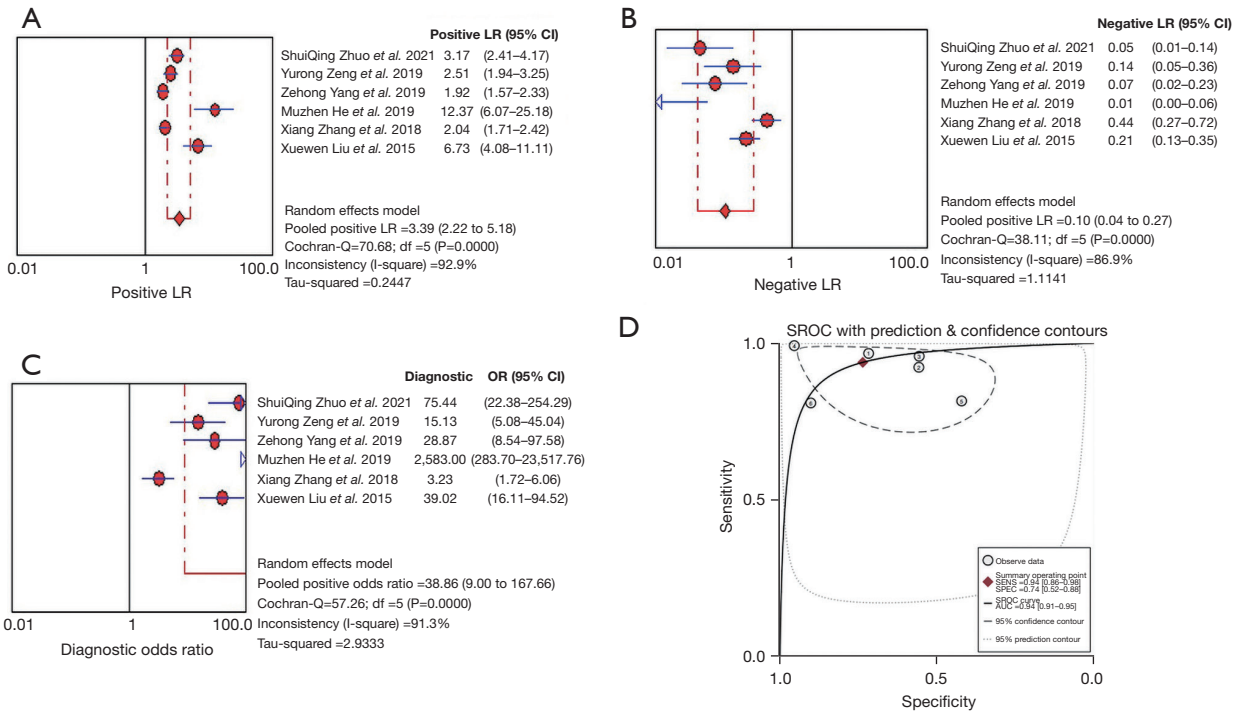

Figure 4 Forest plots of PLR (A), NLR (B), DOR (C), and AUC of SROC (D) for the NIC in the arterial phase combined with the slope in the arterial phase. (A) The combined PLR of NIC in the arterial phase combined with the slope in arterial phase for detecting metastatic lymph nodes was 3.39 (95% CI: 2.22–5.18). (B) The combined NLR of the NIC in the arterial phase combined with the slope in the arterial phase for detecting metastatic lymph nodes was 0.10 (95% CI: 0.04–0.27). (C) The combined DOR of NIC in the arterial phase combined with the slope in the arterial phase for detecting metastatic lymph nodes was 38.86 (95% CI: 9.00–167.66). (D) The AUC of the NIC in the arterial phase combined with the slope in the arterial phase was the largest, with a value of 0.94. LR, likelihood ratio; CI, confidence interval; PLR, positive likelihood ratio; NLR, negative likelihood ratio; DOR, diagnostic odds ratio; AUC, area under curve; SROC, summary receiver operating characteristic; NIC, normalized iodine concentration; SENS, sensitivity; SPEC, specificity.

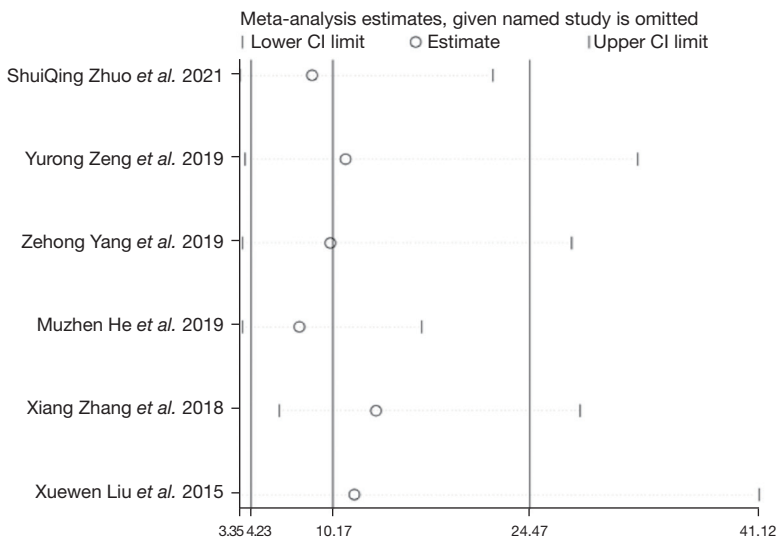

Figure 5 Sensitivity analysis for the NIC in the arterial phase combined with the slope in the arterial phase. CI, confidence interval; NIC, normalized iodine concentration.

Table 4 Meta-regression analysis for each parameter

Parameter	Diagnostic indicators	DECT brand	Blood supply	Contrast flow rate	Study design
IC in AP	Sensitivity	–	–	+	–
	Specificity	–	–	–	–
NIC in AP	Sensitivity	–	–	–	+
	Specificity	–	–	–	–
Slope in AP	Sensitivity	–	–	–	+
	Specificity	–	–	–	–
IC in VP	Sensitivity	–	+	–	–
	Specificity	+	+	+	–
NIC in VP	Sensitivity	–	–	–	+
	Specificity	–	–	–	–
Slope in VP	Sensitivity	–	–	–	+
	Specificity	–	–	–	–
IC in AP + NIC in AP	Sensitivity	+	–	–	–
	Specificity	–	–	–	–
NIC in AP + slope in AP	Sensitivity	–	–	–	+
	Specificity	–	–	–	–
NIC in AP + NIC in VP	Sensitivity	–	+	–	+
	Specificity	–	–	–	–
NIC in AP + slope in VP	Sensitivity	–	–	–	+
	Specificity	–	–	–	–
Slope in AP + NIC in VP	Sensitivity	–	–	–	+
	Specificity	–	–	–	–
Slope in AP + slope in VP	Sensitivity	+	–	–	+
	Specificity	–	–	–	–
IC in VP + NIC in VP	Sensitivity	–	–	–	–
	Specificity	+	+	+	–
Slope in VP + slope in VP	Sensitivity	–	–	+	–
	Specificity	–	–	–	–
NIC in VP + slope in VP	Sensitivity	–	–	–	+
	Specificity	–	–	–	+

"+": significant effect on the heterogeneity; "–": nonsignificant effect on the heterogeneity. IC, iodine concentration; AP, arterial phase; NIC, normalized iodine concentration; VP, venous phase; DECT, dual-energy computed tomography.

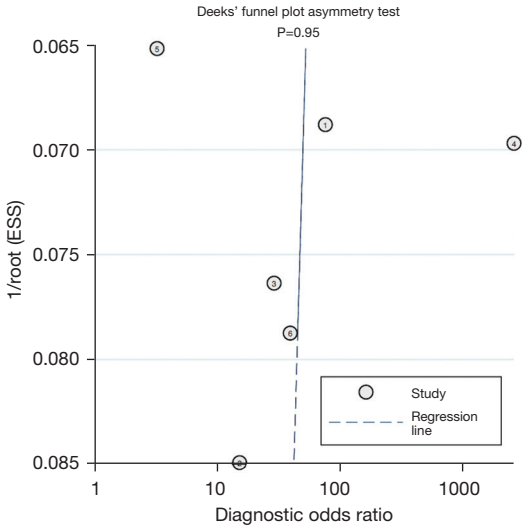

Figure 6 Publication bias. Deeks test was used to evaluate publication bias for NIC in the arterial phase combined with the slope in the arterial phase. ESS, effective sample size; NIC, normalized iodine concentration.

diagnosis of metastatic lymph nodes.

Diagnostic studies are usually more heterogeneous than are other types of studies because of differences in case selection, gold standard settings, and experimental procedures. Based on sensitivity analysis and clinical practice, we then formally evaluated the effect of the following variables on sensitivity and specificity: DECT brand (Siemens *vs.* General Electric Company); blood supply (abundant *vs.* insufficient), contrast flow rate (>3 *vs.* ≤3 mL/s), and study design (prospective *vs.* retrospective). For the NIC in the arterial phase combined with the slope in the arterial phase, meta-regression analysis showed a significant effect of the experimental design on the heterogeneity of sensitivity (P<0.00). These 4 variables also affected the sensitivity and specificity of the remaining partial parameters. In addition, the heterogeneity in this study may also be due to the different sizes of lymph nodes, the different blood supplies to lymph nodes during different periods, the different types of cancer, the different settings of machine parameters, and the different types and doses of contrast agents. In the studies by Li *et al.* (16), Zhao *et al.* (33) and Kato *et al.* (37), the contrast agents used were not described in the text, and the patients included in the study by Zhang *et al.* (31) were all female, which might have contributed to the large heterogeneity observed in these studies.

This meta-analysis had some limitations. While a very extensive literature search was conducted for this study, variables such as different types of cancer, lymph node sizes, machine characteristics, and DECT technologies might have affected diagnostic accuracy. However, this review did not evaluate the combined role of these variables.

Conclusions

With the development and refinement of various imaging techniques, DECT has great clinical significance and application prospects in detecting metastatic and benign lymph nodes. To make the best use of DECT in this respect, it is helpful to combine the two parameters of NIC in the arterial phase and slope in the arterial phase. To further investigate and validate the reliability of the results of this analysis, we need to design prospective cohort studies of high quality, with large sample sizes, homogeneous study populations, homogeneous control populations, and homogeneous detection methods and combine morphological features to model the best combination of parameters to provide clinical guidance for the differential diagnosis of benign and metastatic lymph nodes. In addition, DECT parameters with the best diagnostic performance for each tumor type and the best DECT techniques should also be sought to be able to provide individual guidance for the differentiation of benign and malignant lymph nodes in each patient with cancer, and this should be the focus of further clinical research.

Acknowledgments

Funding: This study received financial support from the Science and Technology Department of Jilin Province (No. 20220203151SF).

Footnote

Reporting Checklist: The authors have completed the PRISMA-DTA reporting checklist. Available at https://qims.amegroups.com/article/view/10.21037/qims-22-527/rc

Conflicts of Interest: All authors have completed the ICMJE uniform disclosure form (available at https://qims.amegroups.com/article/view/10.21037/qims-22-527/coif). All authors reported that this work was supported by the Science and Technology Department of Jilin Province (No. 20220203151SF). The authors have no other conflicts of

interest to declare.

Ethical Statement: The authors are accountable for all aspects of the work in ensuring that questions related to the accuracy or integrity of any part of the work are appropriately investigated and resolved.

References

1. Sung H, Ferlay J, Siegel RL, Laversanne M, Soerjomataram I, Jemal A, Bray F. Global Cancer Statistics 2020: GLOBOCAN Estimates of Incidence and Mortality Worldwide for 36 Cancers in 185 Countries. CA Cancer J Clin 2021;71:209-49.
2. Gillot L, Baudin L, Rouaud L, Kridelka F, Noël A. The pre-metastatic niche in lymph nodes: formation and characteristics. Cell Mol Life Sci 2021;78:5987-6002.
3. Nguyen AT, Luu M, Lu DJ, Hamid O, Mallen-St Clair J, Faries MB, Gharavi NM, Ho AS, Zumsteg ZS. Quantitative metastatic lymph node burden and survival in Merkel cell carcinoma. J Am Acad Dermatol 2021;84:312-20.
4. Kato H, Kanematsu M, Kato Z, Teramoto T, Mizuta K, Aoki M, Makita H, Kato K. Necrotic cervical nodes: usefulness of diffusion-weighted MR imaging in the differentiation of suppurative lymphadenitis from malignancy. Eur J Radiol 2013;82:e28-35.
5. Li J, Fang M, Wang R, Dong D, Tian J, Liang P, Liu J, Gao J. Diagnostic accuracy of dual-energy CT-based nomograms to predict lymph node metastasis in gastric cancer. Eur Radiol 2018;28:5241-9.
6. Okada K, Matsuda M, Tsuda T, Kido T, Murata A, Nishiyama H, Nishiyama K, Yamasawa H, Kamei Y, Kurata M, Fukushima M, Kitazawa R, Mochizuki T. Dual-energy computed tomography for evaluation of breast cancer: value of virtual monoenergetic images reconstructed with a noise-reduced monoenergetic reconstruction algorithm. Jpn J Radiol 2020;38:154-64.
7. Ji GW, Zhang YD, Zhang H, Zhu FP, Wang K, Xia YX, Zhang YD, Jiang WJ, Li XC, Wang XH. Biliary Tract Cancer at CT: A Radiomics-based Model to Predict Lymph Node Metastasis and Survival Outcomes. Radiology 2019;290:90-8.
8. Xie T, Li Y, He G, Zhang Z, Shi Q, Cheng G. The influence of liver fat deposition on the quantification of the liver-iron fraction using fast-kilovolt-peak switching dual-energy CT imaging and material decomposition technique: an in vitro experimental study. Quant Imaging Med Surg 2019;9:654-61.
9. Grillet F, Busse-Coté A, Calame P, Behr J, Delabrousse E, Aubry S. COVID-19 pneumonia: microvascular disease revealed on pulmonary dual-energy computed tomography angiography. Quant Imaging Med Surg 2020;10:1852-62.
10. Weidman EK, Plodkowski AJ, Halpenny DF, Hayes SA, Perez-Johnston R, Zheng J, Moskowitz C, Ginsberg MS. Dual-Energy CT Angiography for Detection of Pulmonary Emboli: Incremental Benefit of Iodine Maps. Radiology 2018;289:546-53.
11. Booz C, Nöske J, Martin SS, Albrecht MH, Yel I, Lenga L, Gruber-Rouh T, Eichler K, D'Angelo T, Vogl TJ, Wichmann JL. Virtual Noncalcium Dual-Energy CT: Detection of Lumbar Disk Herniation in Comparison with Standard Gray-scale CT. Radiology 2019;290:446-55.
12. Zhang W, Zhao S, Pan H, Zhao Y, Zhao X. An iterative reconstruction method based on monochromatic images for dual energy CT. Med Phys 2021;48:6437-52.
13. Hoover KB, Starks AO, Robila V, Riddle DL. Quantitative contrast enhanced dual energy CT to predict avascular necrosis: a feasibility study of proximal humerus fractures. BMC Med Imaging 2021;21:191.
14. Albrecht MH, Vogl TJ, Martin SS, Nance JW, Duguay TM, Wichmann JL, De Cecco CN, Varga-Szemes A, van Assen M, Tesche C, Schoepf UJ. Review of Clinical Applications for Virtual Monoenergetic Dual-Energy CT. Radiology 2019;293:260-71.
15. Chen S, Zhang J, Quan X, Xie Y, Deng X, Zhang Y, Shi S, Liang Z. Diagnostic accuracy of dual-energy computed tomography to differentiate intracerebral hemorrhage from contrast extravasation after endovascular thrombectomy for acute ischemic stroke: systematic review and meta-analysis. Eur Radiol 2022;32:432-41.
16. Li L, Cheng SN, Zhao YF, Wang XY, Luo DH, Wang Y. Diagnostic accuracy of single-source dual-energy computed tomography and ultrasonography for detection of lateral cervical lymph node metastases of papillary thyroid carcinoma. J Thorac Dis 2019;11:5032-41.

17. Cao Y, Zhang J, Bao H, Zhang G, Yan X, Wang Z, Ren J, Chai Y, Zhao Z, Zhou J. Development of a Nomogram Combining Clinical Risk Factors and Dual-Energy Spectral CT Parameters for the Preoperative Prediction of Lymph Node Metastasis in Patients With Colorectal Cancer. Front Oncol 2021;11:689176.
18. McCollough CH, Boedeker K, Cody D, Duan X, Flohr T, Halliburton SS, Hsieh J, Layman RR, Pelc NJ. Principles and applications of multienergy CT: Report of AAPM Task Group 291. Med Phys 2020;47:e881-912.
19. Otrakji A, Digumarthy SR, Lo Gullo R, Flores EJ, Shepard JA, Kalra MK. Dual-Energy CT: Spectrum of Thoracic Abnormalities. Radiographics 2016;36:38-52.
20. Singh R, Sharma A, McDermott S, Homayounieh F, Rastogi S, Flores EJ, Shepard JAO, Gilman MD, Digumarthy SR. Comparison of image quality and radiation doses between rapid kV-switching and dual-source DECT techniques in the chest. Eur J Radiol 2019;119:108639.
21. McInnes MDF, Moher D, Thombs BD, McGrath TA, Bossuyt PM; et al. Preferred Reporting Items for a Systematic Review and Meta-analysis of Diagnostic Test Accuracy Studies: The PRISMA-DTA Statement. JAMA 2018;319:388-96.
22. Wade R, Corbett M, Eastwood A. Quality assessment of comparative diagnostic accuracy studies: our experience using a modified version of the QUADAS-2 tool. Res Synth Methods 2013;4:280-6.
23. Zhuo S, Sun J, Chang J, Liu L, Li S. Dual-source dual-energy thin-section CT combined with small field of view technique for small lymph node in thyroid cancer: a retrospective diagnostic study. Gland Surg 2021;10:1347-58.
24. Zou Y, Zheng M, Qi Z, Guo Y, Ji X, Huang L, Gong Y, Lu X, Ma G, Xia S. Dual-energy computed tomography could reliably differentiate metastatic from non-metastatic lymph nodes of less than 0.5 cm in patients with papillary thyroid carcinoma. Quant Imaging Med Surg 2021;11:1354-67.
25. Yang Z, Zhang X, Fang M, Li G, Duan X, Mao J, Shen J. Preoperative Diagnosis of Regional Lymph Node Metastasis of Colorectal Cancer With Quantitative Parameters From Dual-Energy CT. AJR Am J Roentgenol 2019;213:W17-25.
26. Sun X, Niwa T, Ozawa S, Endo J, Hashimoto J. Detecting lymph node metastasis of esophageal cancer on dual-energy computed tomography. Acta Radiol 2022;63:3-10.
27. Zeng YR, Yang QH, Liu QY, Min J, Li HG, Liu ZF, Li JX. Dual energy computed tomography for detection of metastatic lymph nodes in patients with hepatocellular carcinoma. World J Gastroenterol 2019;25:1986-96.
28. Qiu L, Hu J, Weng Z, Liu S, Jiang G, Cai X. A prospective study of dual-energy computed tomography for differentiating metastatic and non-metastatic lymph nodes of colorectal cancer. Quant Imaging Med Surg 2021;11:3448-59.
29. Wu YY, Wei C, Wang CB, Li NY, Zhang P, Dong JN. Preoperative Prediction of Cervical Nodal Metastasis in Papillary Thyroid Carcinoma: Value of Quantitative Dual-Energy CT Parameters and Qualitative Morphologic Features. AJR Am J Roentgenol 2021;216:1335-43.
30. He M, Lin C, Yin L, Lin Y, Zhang S, Ma M. Value of Dual-Energy Computed Tomography for Diagnosing Cervical Lymph Node Metastasis in Patients With Papillary Thyroid Cancer. J Comput Assist Tomogr 2019;43:970-5.
31. Zhang X, Zheng C, Yang Z, Cheng Z, Deng H, Chen M, Duan X, Mao J, Shen J. Axillary Sentinel Lymph Nodes in Breast Cancer: Quantitative Evaluation at Dual-Energy CT. Radiology 2018;289:337-46.
32. Foust AM, Ali RM, Nguyen XV, Agrawal A, Prevedello LM, Bourekas EC, Boulter DJ. Dual-Energy CT-Derived Iodine Content and Spectral Attenuation Analysis of Metastatic Versus Nonmetastatic Lymph Nodes in Squamous Cell Carcinoma of the Oropharynx. Tomography 2018;4:66-71.
33. Zhao Y, Li X, Li L, Wang X, Lin M, Zhao X, Luo D, Li J. Preliminary study on the diagnostic value of single-source dual-energy CT in diagnosing cervical lymph node metastasis of thyroid carcinoma. J Thorac Dis 2017;9:4758-66.
34. Li X, Meng X, Ye Z. Iodine quantification to characterize primary lesions, metastatic and non-metastatic lymph nodes in lung cancers by dual energy computed tomography: An initial experience. Eur J Radiol 2016;85:1219-23.
35. Liu H, Yan F, Pan Z, Lin X, Luo X, Shi C, Chen X, Wang B, Zhang H. Evaluation of dual energy spectral CT in differentiating metastatic from non-metastatic lymph nodes in rectal cancer: Initial experience. Eur J Radiol 2015;84:228-34.
36. Liu X, Ouyang D, Li H, Zhang R, Lv Y, Yang A, Xie C. Papillary thyroid cancer: dual-energy spectral CT quantitative parameters for preoperative diagnosis of metastasis to the cervical lymph nodes. Radiology 2015;275:167-76.
37. Kato T, Uehara K, Ishigaki S, Nihashi T, Arimoto A, Nakamura H, Kamiya T, Oshiro T, Ebata T, Nagino M.

Clinical significance of dual-energy CT-derived iodine quantification in the diagnosis of metastatic LN in colorectal cancer. Eur J Surg Oncol 2015;41:1464-70.
38. Choi Y, Bin-Manie M, Roh JL, Cho KJ, Lee YS, Choi SH, Nam SY, Kim SY. Metastatic lymph node burden predictive of survival in patients undergoing primary surgery for laryngeal and hypopharyngeal cancer. J Cancer Res Clin Oncol 2019;145:2565-72.
39. Wu H, Dong S, Li X, Shi L, Shao D, Zhang Q, Chen M, Cao Y, Thant M, Huang X. Clinical utility of dual-energy CT used as an add-on to 18F FDG PET/CT in the preoperative staging of resectable NSCLC with suspected single osteolytic metastases. Lung Cancer 2020;140:80-6.
40. Lee SY, Chao-Nan Q, Seng OA, Peiyi C, Bernice WH, Swe MS, Chii WJ, Jacqueline HS, Chee SK. Changes in specialized blood vessels in lymph nodes and their role in cancer metastasis. J Transl Med 2012;10:206.

Cite this article as: Kong D, Chen X, Gao P, Zhao K, Zheng C, Zhou H. Diagnostic accuracy of contrast-enhanced dual-energy computed tomography for detecting metastatic lymph nodes in patients with malignant tumors: a systematic review and meta-analysis. Quant Imaging Med Surg 2023;13(5):3050-3065. doi: 10.21037/qims-22-527

Appendix 1

Search strategy for PubMed

("lymph nodes"[MeSH Terms] OR "lymph node"[Title/Abstract] OR "lymph node"[Title/Abstract] OR "nodes lymph"[Title/Abstract] OR ("lymphatic metastasis"[MeSH Terms] OR "lymphatic metastases"[Title/Abstract] OR "lymph node metastasis"[Title/Abstract] OR "lymph node metastases"[Title/Abstract] OR "metastasis lymph node"[Title/Abstract])) AND ((((("dual"[All Fields] AND ("energie"[All Fields] OR "energies"[All Fields] OR "energy"[All Fields])) OR (("dual"[All Fields] AND ("energie"[All Fields] OR "energies"[All Fields] OR "energy"[All Fields]) AND ("radionuclide imaging"[MeSH Terms] OR ("radionuclide"[All Fields] AND "imaging"[All Fields]) OR "radionuclide imaging"[All Fields] OR "scanning"[All Fields] OR "scan s"[All Fields] OR "scanned"[All Fields] OR "scannings"[All Fields] OR "scans"[All Fields])) AND ("projection"[MeSH Terms] OR "forecasting"[MeSH Terms]))) AND ("CT"[Title/Abstract] OR "computed tomograph*"[Title/Abstract] OR "tomography, x–ray computed"[MeSH Terms])) OR "dect"[Title/Abstract] OR "spectral ct"[Title/Abstract])

Search strategy for Cochrane

Search Name:
Date Run: 01/10/2022 08:15:55
Comment:

ID	Search	Hits
#1	MeSH descriptor: [Lymphatic Metastasis] explode all trees	1920
#2	(Lymphatic Metastases):ti,ab,kw OR (Lymph Node Metastasis):ti,ab,kw OR (Lymph Node Metastases):ti,ab,kw OR (Metastasis, Lymph Node):ti,ab,kw (Word variations have been searched)	5609
#3	#1or#2	6207
#4	MeSH descriptor: [Lymph Nodes] explode all trees	907
#5	(Lymph Node):ti,ab,kw OR (Node, Lymph):ti,ab,kw OR (Nodes, Lymph):ti,ab,kw (Word variations have been searched)	12965
#6	#4or#5	12971
#7	#3or#6	13707
#8	MeSH descriptor: [Tomography, Emission-Computed] explode all trees	2652
#9	(ct):ti,ab,kw OR (computed tomograph):ti,ab,kw (Word variations have been searched)	81765
#10	#8or#9	83800
#11	(dual energy):ti,ab,kw (Word variations have been searched)	6153
#12	#10and#11	828
#13	(dect):ti,ab,kw OR (spectral ct):ti,ab,kw (Word variations have been searched)	295
#14	#12or#13	1042
#15	#7and#14	3

Search strategy for Embase

Embase Session Results

No.	Query	Results
#19	#18 AND #10	235
#18	#14 OR #17	395,622
#17	#15 OR #16	282,888
#16	'lymph nodes':ab,ti OR 'node, lymph':ab,ti OR 'nodes, lymph':ab,ti	168,824
#15	'lymph node'/exp	208,033
#14	#11 OR #13	171,888
#13	'lymphatic metastasis':ab,ti OR 'lymphatic metastases':ab,ti OR 'lymph node metastases':ab,ti OR 'metastasis, lymph node':ab,ti	31,605
#11	'lymph node metastasis'/exp	165,753
#10	#4 OR #9	15,209
#9	#3 AND #8	14,377
#8	'dual energy'	59,399
#4	'dural energy computer assisted tomography' OR 'dect' OR 'spectral ct'	3,650
#3	#1 OR #2	1,834,338
#2	'ct' OR 'computer tomography$'	1,022,897
#1	'computer assisted tomography'/exp	1,313,207

https://dx.doi.org/10.21037/qims-22-527

Appendix 2 Specific reasons for exclusion at the full-text screening stage

N	First author	Year	Title	Journal	Reasons for exclusion
1	Yang *et al.*	2022	Radiomics profiling identifies the value of CT features for the preoperative evaluation of lymph node metastasis in papillary thyroid carcinoma	*Diagnostics*	Unable to extract data: unable to obtain diagnostic indicators for individual parameters
2	Xu *et al.*	2022	Iodine maps from dual-energy CT to predict extrathyroidal extension and recurrence in papillary thyroid cancer based on a radiomics approach	*American Journal of Neuroradiology*	Wrong outcome: prediction of tumor recurrence
3	Hong *et al.*	2022	Value of dual-layer spectral detector CT in preoperative prediction of lymph node metastasis of gastric cancer	*Zhonghua Yi Xue Za Zhi*	Non–English language literature
4	Li *et al.*	2021	Histological subtypes of solid-dominant invasive lung adenocarcinoma: differentiation using dual-energy spectral CT	*Clinical Radiology*	Wrong outcome: prediction of tumor recurrence
5	Zeng *et al.*	2021	Decoupling convolution network for characterizing the metastatic lymph nodes of breast cancer patients	*Medical Physics*	Unable to extract data: unable to obtain diagnostic indicators for individual parameters
6	Zou *et al.*	2021	A new prediction model for lateral cervical lymph node metastasis in patients with papillary thyroid carcinoma: based on dual-energy CT	*European Journal of Radiology*	Unable to extract data: unable to obtain diagnostic indicators for individual parameters
7	Zhou *et al.*	2021	Radiomics from primary tumor on dual-energy CT derived iodine maps can predict cervical lymph node metastasis in papillary thyroid cancer	*Academic Radiology*	Unable to extract data: unable to obtain diagnostic indicators for individual parameters
8	Wang *et al.*	2021	Dual energy CT image prediction on primary tumor of lung cancer for nodal metastasis using deep learning	*Computerized Medical Imaging and Graphics*	Unable to extract data: unable to obtain diagnostic indicators for individual parameters
9	Takumi *et al.*	2021	Usefulness of dual-layer spectral CT in follow-up examinations: diagnosing recurrent squamous cell carcinomas in the head and neck	*Japanese Journal of Radiology*	Wrong outcome: prediction of tumor recurrence
10	Martin *et al.*	2021	Prospective evaluation of the first integrated positron emission Tomography/dual-energy computed tomography system in patients with lung cancer	*Journal of Thoracic Imaging*	Wrong outcome: not a diagnostic accuracy study
11	Le *et al.*	2021	CT features predictive of nodal positivity at surgery in pancreatic cancer patients following neoadjuvant therapy in the setting of dual energy CT	*Abdominal Radiology*	Unable to extract data: no related parameters
12	Kupik *et al.*	2021	A comparison study of dual-energy spectral CT and 18F-FDG PET/CT in primary tumors and lymph nodes of lung cancer	*Diagn Interv Radiol*	Wrong outcome: not a diagnostic accuracy study
13	Cao *et al.*	2021	Development of a nomogram combining clinical risk factors and dual-energy spectral CT parameters for the preoperative prediction of lymph node metastasis in patients with colorectal cancer	*Frontiers in Oncology*	Unable to extract data: unable to obtain diagnostic indicators for individual parameters
14	Xu *et al.*	2021	Integrating CT image features and quantitative dual-energy CT parameters for diagnosing metastatic lymph nodes from papillary thyroid carcinoma	*Chinese Journal of Radiology*	Non–English language literature
15	An *et al.*	2021	Deep learning radiomics of dual-energy computed tomography for predicting lymph node metastases of pancreatic ductal adenocarcinoma	*European Journal of Nuclear Medicine and Molecular Imaging*	Unable to extract data: unable to obtain diagnostic indicators for individual parameters
16	Zhou *et al.*	2020	Radiomics analysis of dual-energy CT-derived iodine maps for diagnosing metastatic cervical lymph nodes in patients with papillary thyroid cancer	*European Radiology*	Unable to extract data: radiomics studies
17	Wang *et al.*	2020	Dual-energy CT in the differentiation of stage T1 nasopharyngeal carcinoma and lymphoid hyperplasia	*European Radiology*	Unable to extract data: unable to obtain diagnostic indicators for individual parameters
18	Liu *et al.*	2020	A study of radiomics parameters from dual-energy computed tomography images for lymph node metastasis evaluation in colorectal mucinous adenocarcinoma	*Medicine*	Unable to extract data: unable to obtain diagnostic indicators for individual parameters
19	Li *et al.*	2020	Dual-energy CT–based deep learning radiomics can improve lymph node metastasis risk prediction for gastric cancer	*European Radiology*	Unable to extract data: radiomics studies
20	Kim *et al.*	2020	Application of dual-energy spectral computed tomography to thoracic oncology imaging	*Korean J Radiol*	Nonoriginal article

Appendix 2 (*continued*)

https://dx.doi.org/10.21037/qims-22-527

Appendix 2 (*continued*)

N	First author	Year	Title	Journal	Reasons for exclusion
21	Yang *et al.*	2018	Dual-source CT iodine concentration and Overlay value in diagnosis of different degree gastric cancer and metastatic lymph nodes	*Chinese Journal of Medical Imaging Technology*	Non–English language literature
22	Seidler *et al.*	2019	Dual-Energy CT texture analysis with machine learning for the evaluation and characterization of cervical lymphadenopathy	*Computational and Structural Biotechnology Journal*	Unable to extract data: unable to obtain diagnostic indicators for individual parameters
23	Forghani *et al.*	2019	Head and neck squamous cell carcinoma: prediction of cervical lymph node metastasis by dual-energy CT texture analysis with machine learning	*European Radiology*	Unable to extract data: unable to obtain diagnostic indicators for individual parameters
24	Huang *et al.*	2019	Dual-energy CT iodine image for evaluation of cervical lymph node metastatic potential in papillary thyroid microcarcinoma	*Chinese Journal of Radiology*	Non–English language literature
25	Rizzo *et al.*	2019	Metastatic and non-metastatic lymph nodes: quantification and different distribution of iodine uptake assessed by dual-energy CT	*European Radiology*	Unable to extract data: unable to obtain diagnostic indicators for individual parameters
26	Morgan *et al.*	2019	The role of dual-energy computed tomography in assessment of abdominal oncology and beyond	*Radiol Clin North Am*	Nonoriginal article
27	Li *et al.*	2019	Diagnostic accuracy of dual-energy CT-based nomograms to predict lymph node metastasis in gastric cancer	*European Radiology*	Unable to extract data: unable to obtain diagnostic indicators for individual parameters
28	Zheng *et al.*	2017	Dual energy CT in diagnosis of central cervical metastatic lymph nodes in patients with papillary thyroid cancer	*Chinese Journal of Medical Imaging Technology*	Non–English language literature
29	Hokamp *et al.*	2018	Verbesserte Darstellung intraspinaler Lymphome mittels virtuell-monoenergetischen Rekonstruktionen der Dual-Energy-CT	*Rofo*	Non–English language literature
30	Yang *et al.*	2016	GSI quantitative parameters: Preoperative diagnosis of metastasis lymph nodes in lung cancer	*Chinese Journal of Lung Cancer*	Non–English language literature
31	Yang *et al.*	2016	Dual source CT dual-energy imaging technology in differential diagnosis of the metastatic and reactive hyperplastic lymph nodes in patients with colorectal cancer	*Chinese Journal of Medical Imaging Technology*	Non–English language literature
32	Yang *et al.*	2016	Differentiation of malignant cervical lymphadenopathy by dual-energy CT: a preliminary analysis	*Scientific reports*	Unable to extract data: unable to obtain diagnostic indicators for individual parameters
33	Wang *et al.*	2015	Application of single-source dual-energy spectral CT in differentiating lymphoma and metastatic lymph nodes in the head and neck	*Journal: Chinese Journal of Oncology*	Non–English language literature
34	Liang *et al.*	2015	A retrospective study of dual-energy CT for clinical detecting of metastatic cervical lymph nodes in laryngeal and hypopharyngeal squamous cell carcinoma	*Acta Oto-Laryngologica*	Unable to extract data: unable to obtain diagnostic indicators for individual parameters
35	Fu *et al.*	2015	Dua-energy virtual noncontrast imaging in diagnosis of cervical metastasis lymph nodes	*Journal of Cancer Research and Therapeutics*	Unable to extract data: Unable to obtain diagnostic indicators for individual parameters
36	Liu *et al.*	2014	MSCT in diagnosis of non-functioning cystic neuroendocrine tumors of pancreas	*Chinese Journal of Interventional Imaging and Therapy*	Non–English language literature
37	Baxa *et al.*	2014	Dual-phase dual-energy CT in patients with lung cancer: assessment of the additional value of iodine quantification in lymph node therapy response	*European Radiology*	Unable to extract data: unable to obtain diagnostic indicators for individual parameters
38	Pei *et al.*	2013	Evaluation of advanced gastric carcinoma with monoenergetic spectrum curve of dual-source dual-energy computed tomography	*Chinese Medical Sciences Journal*	Nonoriginal article
39	Wang *et al.*	2013	Dual-energy CT in differential diagnosis of lymphoma and metastatic lymph nodes	*Chinese Journal of Medical Imaging Technology*	Non–English language literature

CT, computed tomography; MSCT, multislice computed tomography

https://dx.doi.org/10.21037/qims-22-527

Appendix 3

Table S1 Main findings of included studies for IC in the arterial phase

Study ID	Total	True positives	False positives	False negatives	True negatives	Sensitivity	Specificity
Zou *et al.* 2021	359	102	62	37	158	73.63%	71.94%
Zhuo *et al.* 2021	216	78	17	14	107	84.80%	86.30%
Sun *et al.* 2020	51	23	4	11	13	67.80%	76.40%
Zeng *et al.* 2019	156	36	29	16	75	68.60%	72.00%
Li *et al.* 2016	40	16	7	4	13	80%	65%
Kato *et al.* 2015	81	30	5	5	41	84.80%	88.60%

IC, iodine concentration.

Table S2 Main findings of the included studies for NIC in the arterial phase

Study ID	Total	True positives	False positives	False negatives	True negatives	Sensitivity	Specificity
Zhuo *et al.* 2021	216	76	17	16	107	82.60%	86.30%
Sun *et al.* 2020	51	32	9	2	8	94.10%	47.10%
Zeng *et al.* 2019	156	38	27	14	77	72.80%	73.90%
Yang *et al.* 2019	178	63	36	9	70	87.50%	66.00%
He *et al.* 2019	212	112	3	12	85	90.30%	96.60%
Zhang *et al.* 2018	337	41	104	35	157	54%	60.20%
Li *et al.* 2016	40	15	5	5	15	75%	75%
Liu *et al.* 2015	175	38	4	25	108	60.30%	96.40%
Liu *et al.* 2015	152	39	38	21	54	64.40%	58.30%
Kato *et al.* 2015	81	29	9	6	37	82.60%	81.00%

NIC, normalized iodine concentration.

Table S3 Main findings of the included studies for slope in the arterial phase

Study ID	Total	True positives	False positives	False negatives	True negatives	Sensitivity	Specificity
Zhuo *et al.* 2021	216	75	21	17	103	81.50%	83.10%
Qiu *et al.* 2021	150	67	23	17	43	80.30%	65.48%
Zeng *et al.* 2019	156	38	25	14	79	73.80%	75.60%
Yang *et al.* 2019	178	52	17	20	89	72.20%	84.00%
He *et al.* 2019	212	109	1	15	87	87.90%	98.80%
Zhang *et al.* 2018	337	46	78	30	183	60%	70.10%
Liu *et al.* 2015	175	33	7	30	105	52.40%	93.80%

Table S4 Main findings of the included studies for IC in the venous phase

Study ID	Total	True positives	False positives	False negatives	True negatives	Sensitivity	Specificity
Zhuo *et al.* 2021	216	74	27	18	97	80.40%	78.20%
Wu *et al.* 2021	206	44	19	36	107	55.00%	84.90%
Sun *et al.* 2020	51	27	3	7	14	79.40%	82.40%
Zeng *et al.* 2019	156	43	18	9	86	81.90%	82.40%
Li *et al.* 2019	99	61	2	9	27	87.10%	93.10%
Foust *et al.* 2018	29	11	4	2	12	84.60%	75%
Zhao *et al.*2017	136	85	3	17	31	83.30%	91.20%
Kato *et al.* 2015	81	30	5	5	41	87.00%	88.60%

IC, iodine concentration.

https://dx.doi.org/10.21037/qims-22-527

Table S5 Main findings of the included studies for NIC in the venous phase

Study ID	Total	True positives	False positives	False negatives	True negatives	Sensitivity	Specificity
Zhuo *et al.* 2021	216	74	37	18	87	80.40%	70.20%
Wu *et al.* 2021	206	50	18	30	108	62.50%	85.70%
Sun *et al.* 2020	51	24	3	10	14	70.60%	82.40%
Zeng *et al.* 2019	156	44	17	8	87	83.90%	84.10%
Yang *et al.* 2019	178	60	29	12	77	83.30%	72.60%
Li *et al.* 2019	99	68	7	2	22	97.10%	75.90%
He *et al.* 2019	212	108	18	16	70	87.10%	79.50%
Zhang *et al.* 2018	337	55	75	21	186	73%	71.30%
Zhao *et al.*2017	136	98	8	4	26	96.10%	76.50%
Liu *et al.* 2015	175	38	15	25	97	60.30%	86.60%
Liu *et al.* 2015	152	45	28	15	64	75.50%	70.00%
Kato *et al.* 2015	81	31	6	4	40	89.10%	86.80%

NIC, normalized iodine concentration.

Table S6 Main findings of the included studies for slope in the venous phase

Study ID	Total	True positives	False positives	False negatives	True negatives	Sensitivity	Specificity
Zhuo *et al.* 2021	216	62	23	30	101	67.40%	81.50%
Wu *et al.* 2021	206	42	15	38	111	52.50%	88.10%
Qiu *et al.* 2021	150	47	12	37	54	56.06%	82.14%
Zeng *et al.* 2019	156	43	17	9	87	81.80%	84.10%
Yang *et al.* 2019	178	49	25	23	81	68.00%	76.40%
Li *et al.* 2019	99	64	4	6	25	91.40%	86.20%
He *et al.* 2019	212	102	4	22	84	82.30%	95.50%
Zhang *et al.* 2018	337	50	6	26	255	66%	97.70%
Foust *et al.* 2018	29	12	8	1	8	92.30%	50%
Zhao *et al.*2017	136	90	6	12	28	88.20%	82.40%
Liu *et al.* 2015	175	39	10	24	102	62.00%	91.10%

Table S7 Main findings of the included studies for IC in the arterial phase combined with NIC in the arterial phase

Study ID	Total	True positives	False positives	False negatives	True negatives	Sensitivity	Specificity
Zhuo *et al.* 2021	216	87	47	5	77	95.10%	62.10%
Sun *et al.* 2020	51	34	11	0	6	98.70%	36.00%
Zeng *et al.* 2019	156	28	9	24	95	91.50%	53.20%
Li *et al.* 2016	40	19	10	1	10	95.00%	48.80%
Kato *et al.* 2015	81	34	13	1	33	97.40%	71.80%

IC, iodine concentration; NIC, normalized iodine concentration.

Table S8 Main findings of the included studies for NIC in the arterial phase combined with slope in the arterial phase

Study ID	Total	True positives	False positives	False negatives	True negatives	Sensitivity	Specificity
Zhuo *et al.* 2021	216	89	35	3	89	96.80%	71.70%
Zeng *et al.* 2019	156	48	46	4	58	92.90%	55.90%
Yang *et al.* 2019	178	69	47	3	59	96.50%	55.40%
He *et al.* 2019	212	123	4	1	84	98.80%	95.40%
Zhang *et al.* 2018	337	62	151	14	110	81.60%	42.20%
Liu *et al.* 2015	175	51	11	12	101	81.10%	90.40%

NIC, normalized iodine concentration.

https://dx.doi.org/10.21037/qims-22-527

Table S9 Main findings of the included studies for NIC in the arterial phase combined with NIC in the venous phase

Study ID	Total	True positives	False positives	False negatives	True negatives	Sensitivity	Specificity
Zhuo *et al.* 2021	216	89	49	3	75	96.60%	60.60%
Sun *et al.* 2020	51	33	10	1	7	98.30%	38.80%
Zeng *et al.* 2019	156	50	39	2	65	95.60%	62.10%
Yang *et al.* 2019	178	71	55	1	51	98.00%	47.90%
He *et al.* 2019	212	122	20	2	68	98.70%	76.80%
Zhang *et al.* 2018	337	67	149	9	112	87.60%	42.90%
Liu *et al.* 2015	152	55	54	5	38	91.30%	40.80%
Liu *et al.* 2015	175	53	18	10	94	84.20%	83.50%
Kato *et al.* 2015	81	34	14	1	32	98.10%	70.30%

NIC, normalized iodine concentration.

Table S10 Main findings of the included studies for NIC in the arterial phase combined with slope in the venous phase

Study ID	Total	True positives	False positives	False negatives	True negatives	Sensitivity	Specificity
Zhuo *et al.* 2021	216	87	37	5	87	94.30%	70.30%
Zeng *et al.* 2019	156	49	39	3	65	95.00%	62.10%
Yang *et al.* 2019	178	69	53	3	53	96.00%	50.40%
He *et al.* 2019	212	122	7	2	81	98.30%	92.30%
Zhang *et al.* 2018	337	64	108	12	153	84.40%	58.80%
Liu *et al.* 2015	175	53	14	10	98	84.90%	87.70%

NIC, normalized iodine concentration.

Table S11 Main findings of the included studies for slope in the arterial phase combined with NIC in the venous phase.

Study ID	Total	True positives	False positives	False negatives	True negatives	Sensitivity	Specificity
Zhuo *et al.* 2021	216	89	52	3	72	96.40%	58.30%
Zeng *et al.* 2019	156	50	38	2	66	95.80%	63.60%
Yang *et al.* 2019	178	69	41	3	65	95.40%	61.00%
He *et al.* 2019	212	122	19	2	69	98.40%	78.50%
Zhang *et al.* 2018	337	68	130	8	131	89.20%	50.00%
Liu *et al.* 2015	175	51	21	12	91	81.10%	81.20%

NIC, normalized iodine concentration.

Table S12 Main findings of the included studies for slope in the arterial phase combined with slope in the venous phase

Study ID	Total	True positives	False positives	False negatives	True negatives	Sensitivity	Specificity
Zhuo *et al.* 2021	216	86	40	6	84	94.00%	67.70%
Qiu *et al.* 2021	150	77	31	7	35	91.30%	53.40%
Zeng *et al.* 2019	156	50	38	2	66	95.20%	63.40%
Yang *et al.* 2019	178	66	38	6	68	91.10%	64.20%
He *et al.* 2019	212	121	5	3	83	97.80%	94.30%
Zhang *et al.* 2018	337	66	82	10	179	86.40%	68.50%
Liu *et al.* 2015	175	52	16	11	96	81.90%	85.50%

https://dx.doi.org/10.21037/qims-22-527

Table S13 Main findings of the included studies for IC in the venous phase combined with NIC in the venous phase.

Study ID	Total	True positives	False positives	False negatives	True negatives	Sensitivity	Specificity
Zhuo *et al.* 2021	216	89	56	3	68	96.20%	54.90%
Wu *et al.* 2021	206	66	34	14	92	83.10%	72.80%
Sun *et al.* 2020	51	32	5	2	12	93.90%	67.90%
Zeng *et al.* 2019	156	50	32	2	72	97.00%	69.30%
Li *et al.* 2019	99	70	8	0	21	99.60%	70.70%
Zhao *et al.*2017	136	101	10	1	24	99.30%	69.80%
Kato *et al.* 2015	81	35	11	0	35	98.60%	76.90%

IC, iodine concentration; NIC, normalized iodine concentration.

Table S14 Main findings of the included studies for IC in the venous phase combined with slope in the venous phase

Study ID	Total	True positives	False positives	False negatives	True negatives	Sensitivity	Specificity
Zhuo *et al.* 2021	216	86	45	6	79	93.60%	63.70%
Wu *et al.* 2021	206	63	32	17	94	78.60%	74.80%
Zeng *et al.* 2019	156	50	32	2	72	96.70%	69.30%
Li *et al.* 2019	99	69	6	1	23	98.90%	80.20%
Foust *et al.* 2018	29	13	10	0	6	98.80%	35.00%
Zhao *et al.*2017	136	100	8	2	26	98.00%	75.10%

IC, iodine concentration.

Table S15 Main findings of the included studies for NIC in the venous phase combined with slope in the venous phase

Study ID	Total	True positives	False positives	False negatives	True negatives	Sensitivity	Specificity
Zhuo *et al.* 2021	216	86	53	6	71	93.60%	57.00%
Wu *et al.* 2021	206	66	29	14	97	82.20%	77.10%
Zeng *et al.* 2019	156	50	30	2	74	97.00%	70.70%
Yang *et al.* 2019	178	68	47	4	59	94.70%	55.50%
Li *et al.* 2019	99	70	10	0	19	99.80%	65.40%
He *et al.* 2019	212	121	21	3	67	97.70%	75.90%
Zhang *et al.* 2018	337	69	79	7	182	90.80%	69.70%
Zhao *et al.*2017	136	101	13	1	21	99.50%	63.00%
Liu *et al.* 2015	175	53	24	10	88	84.90%	78.80%

NIC, normalized iodine concentration.

https://dx.doi.org/10.21037/qims-22-527